

Study of the Effect of Temperature on the Galvanic Corrosion Between Alloy 31 Base Metal And Its Weld in Polluted Phosphoric Acid

E. Blasco-Tamarit¹, D.M. García-García¹, J. García-Antón^{1,*}, A. Guenbour²

¹ Ingeniería Electroquímica y Corrosión (IEC). Departamento de Ingeniería Química y Nuclear. Universidad Politécnica de Valencia, Spain,

² Laboratory Corrosion-Electrochimie, Faculty of Sciences, University Mohammed V-Agdal, Rabat (Morocco)

*E-mail: jgarciaa@iqn.upv.es

Received: 21 July 2011 / Accepted: 29 October 2011 / Published: 1 December 2011

This work studies the influence of the solution temperature on the corrosion resistance of a high alloyed austenitic stainless steel (UNS N08031) used as Base Metal (BM), the Heat Affected Zone (HAZ) and the Weld Metal (WM) obtained by the Gas Tungsten Arc Welding technique using a Nickel-base alloy (UNS N06059) as filler metal (GTAW). Electrochemical tests were carried out in a 5.5 M polluted phosphoric acid solution with 0.03 wt% (380 ppm) of chloride ions and 2 wt% of H₂SO₄ at 25, 40, 60 and 80° C. The potentiodynamic curves of the materials were registered in each condition under study and electrochemical parameters such as E_{corr}, i_{corr}, E_b and i_p were obtained. The galvanic corrosion generated between the BM-HAZ and HAZ-WM pairs was also analysed by means of the Mixed Potential Theory. The lower E_b and (E_b-E_{corr}) values and higher i_p values obtained at higher temperatures indicate that the properties of the passive film formed degraded with temperature. The welding process modifies the characteristics of the passive film, deteriorating them and favouring the loss of passivity of the WM with respect to the BM, as shown by the lowest E_b values and highest i_p values of the WM.

Keywords: Steels; Anodic Polarization; Galvanic Corrosion; Passivity; Weld

1. INTRODUCTION

Industrial phosphoric acid solutions are chemically complex and their analysis changes from one plant to another, depending on the quality of the phosphate rocks and the process used in their manufacture. Phosphoric acid in pure state is not very corrosive compared to nitric or sulphuric acids. Phosphoric acid is manufactured by the wet process. In this process the phosphate rocks are attacked

with sulphuric acid. This technique causes severe corrosion problems due to the presence of impurities such as chlorides, fluorides and sulphides [1]. It has long been known that these impurities increase the corrosiveness of the acid [2-4], but it is also known that certain impurities reduce it, such as iron, aluminium and magnesium cations [5].

Materials used in this environment must have good chemical and mechanical resistance. These two characteristics are not always easy to obtain and we have to make compromises between these properties [6]. In this sense, highly alloyed austenitic stainless steels are a good choice to be used in phosphoric media, since they have excellent corrosion and heat resistance with good mechanical properties over a wide range of temperatures. In this work a highly alloyed austenitic stainless steel (UNS 08031) was used as base metal.

The major disadvantage of these new alloys is their high cost compared with baseline stainless steels such as 300 series SS, due to the higher percentage of alloying elements as Cr, Ni and Mo, as well as the complexity of the manufacturing process [7]. These alloys can present pitting corrosion [8-13] and its corrosion behaviour can be deteriorate due to the effect of electrolyte flows [14, 15].

On the other hand, the equipment used in the phosphoric industry is manufactured with different materials; as a consequence, the formation of galvanic pairs may increase corrosion problems. Furthermore, the manufacture of components requires the use of welding. Welding can strongly alter the microstructure of materials by the heat treatment, producing local variations in material composition and structures which can result in sensitisation to materials. In fact, welds are recognised as zones which are particularly sensitive to corrosion [16]. If the weld metal has poorer corrosion resistance than the stainless steel base metal, the attack will concentrate on the weld metal. The filler metals for the welds of corrosion resistant alloys are usually over-alloyed in order to compensate the loss of alloying elements by the welding fume and to protect the local area of low composition due to the segregation in the welds [17, 18]. Also, these filler metals should have good enough mechanical and metallurgical properties to satisfy the requirement of the physical properties in the weld. Therefore, new filler metals need to have both good physical properties and good corrosion resistance.

The objective of the present work is to study the influence of temperature on the corrosion resistance of a highly alloyed austenitic stainless steel used as Base Metal (BM), the Heat Affected Zone (HAZ) and the Weld Metal (WM) obtained by the gas tungsten arc welding technique (GTAW) in 5.5 M polluted phosphoric acid solutions with 0.03 wt% (380 ppm) of chloride ions and 2 wt% of H₂SO₄, which are impurities characteristic of the phosphoric acid obtained by the wet process in industry, as well as to evaluate the galvanic corrosion generated between the BM-HAZ and HAZ-WM pairs. A previous study was conducted by authors related to the corrosion behaviour of these materials in a 5.5 M pure phosphoric acid solution, without these impurities [19].

2. EXPERIMENTAL

2.1. Materials and solution

The materials tested were Alloy 31 (UNS N08031) austenitic stainless steels, used as Base Metal (BM), the Weld Metal (WM) obtained by GTAW (Gas Tungsten Arc Welding Technique)

welding using a Nickel-base alloy (Alloy 59 (UNS N06059)) as filler metal, and the Heat Affected Zone (HAZ). Material compositions are shown in Table 1.

Table 1. Materials composition

Material	Cr	Ni	N	C	P	Mn	S	Si	Cu	Mo	Fe	Co	Al
UNS N08031	26.75	31.85	0.193	0.005	0.017	1.5	0.002	0.1	1.21	6.60	31.43	-	-
UNS N06059	22.65	60.58	-	0.002	0.003	0.15	0.002	0.03	-	15.40	0.58	0.04	0.16

The materials tested were obtained from two plates of Alloy 31 joined by welding (GTAW) using Alloy 59 as filler metal. Three zones were identified on the plate obtained after welding: WM, HAZ and BM (Figure 1a). Samples from each zone were obtained as cylindrical disks (10 mm in diameter) by the method of water jets cutting and they were used as working electrodes, with an exposed area of 0.785 cm². The WM specimens were obtained from the weld pool shown in Figure 1b. As the HAZ is close to the weld, it is affected by the heat treatment used in the welding process. The BM specimens were obtained from a zone far away from the weld pool. The samples were abraded up to 4000 grit emery paper. Subsequently the electrode was rinsed with distilled water and alcohol and was air-dried. The studied materials were examined by Optical Microscopy and SEM (Scanning Electronic Microscopy) for reveal their microstructure.

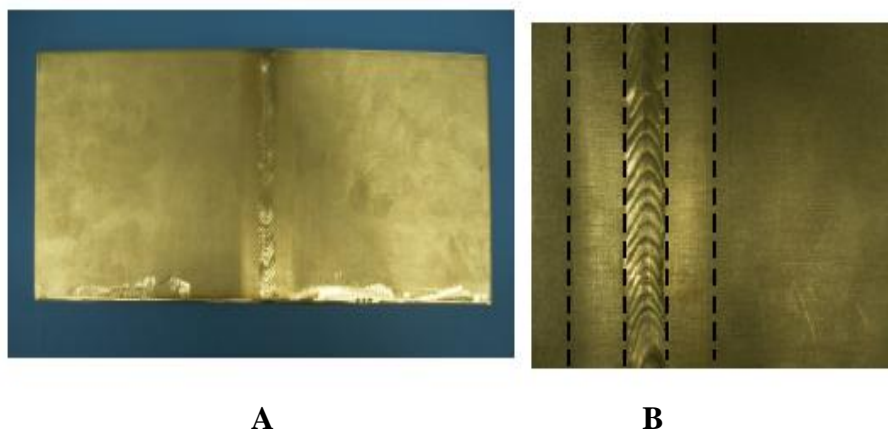


Figure 1. Plate obtained after the welding of two plates of Alloy 31 with filler material Alloy 59. The delimited zones correspond to the three materials, BM, HAZ and WM (a); Figure (b) shows the weld pool and the zone from which the HAZ specimens were obtained.

All measurements were performed in 5.5 M polluted phosphoric acid solutions with 0.03 wt% (380 ppm) of chloride ions and 2 wt% of H₂SO₄. This solution has the same characteristics of phosphoric acid obtained by the wet process in the industry.

2.2. Electrochemical measurements

Potentiodynamic anodic polarisation measurements were developed according to a modification of ASTM G5 test [20] with a potentiostat. Tests were conducted in a three-electrode cell with a Ag/AgCl 3M KCl electrode as reference electrode and a platinum wire as counter electrode. The electrolyte was purged with purified nitrogen gas during 20 min before the test to deaerate the solution. A nitrogen atmosphere over the liquid surface was maintained during the whole test. The experimental device [21, 22] consists of two elements: the electrochemical unit and the image acquisition section. This method allows the real-time visualisation of the corrosion phenomena on the materials simultaneously to the electrochemical data acquisition without disturbing the electrochemical system.

Prior to each anodic polarisation measurement, the open circuit potential was measured for 1 hour in the test solutions. The average value of the potentials recorded during the last 300 seconds was the OCP value. The potentiodynamic polarisation curves were carried out from -200 mV with respect to OCP to the anodic direction with a scan rate of 0.1667 mV/s. Current corrosion density (i_{corr}) and corrosion potential (E_{corr}) were obtained from the potentiodynamic curves to study the general electrochemical behaviour of the materials [23]. The potential at which the current density exceeded $100 \mu\text{A}/\text{cm}^2$ was defined as breakdown potential (E_b), and represent the potential at which the current starts to rise significantly over a small shift in potential indicating a loss of passivity. Passivation current density (i_p) was also calculated. At least three experiments were carried out for all specimens.

Temperature influence on the corrosion behaviour of the alloys was also analysed. Temperature was controlled by regulating the heater power with a Compatible Control Thermostat. The working temperatures were kept constant at 25, 40, 60 and 80° C during the whole tests.

The galvanic corrosion between BM-HAZ and HAZ-BM was evaluated from the polarisation curves by superimposing the potentiodynamic curves of both materials. The predicted mixed potential (E_M) and the galvanic current density (i_G) of the pair were estimated from the intersection point of the anodic curve of one alloy with the cathodic curve of the other one, according to the mixed potential theory [24]. The mixed potential theory has been widely used to study galvanic corrosion [25-28] and, in particular, the galvanic corrosion behaviour of nonwelded/welded couples [29-33].

3. RESULTS AND DISCUSSION

3.1. Microstructure characterisation

To analyse the effect of welding on the microstructure of BM and HAZ, and consequently on galvanic corrosion, a microstructural analysis of the materials was performed by means of optical microscopy and Scanning Electron Microscopy (SEM).

Samples of BM and HAZ were electrolytically etched with Bell and Sonon's reagent (60% HNO_3). Etching was performed at 70 mA during 120s. The microstructure of WM was revealed in 10% oxalic acid and etching was performed at 6V during 90s [34, 35].

Images of the microstructures of the materials are reported in a previous work conducted by authors, since the studied materials were the same BM, HAZ and WM [19]. That paper shows that the microstructure of BM, revealed a single austenitic phase with equiaxed grains and many twins which formed during grain growth or during deformation in the manufacturing process of the Alloy 31. This is the typical microstructure of an austenitic stainless steel. In the HAZ specimen, the same microstructure is observed, although grains are slightly larger than those of the BM. The microstructure of the WM revealed a dendritic microstructure, characteristic of solidification processes of metals.

A different etching (immersion in 15 ml nitric acid- 85 ml methanol and 85 ml water during 120 s [35]) was employed to reveal the Cr and Mo accumulations on the grain boundaries. An Energy Dispersive X-ray analysis (EDX) was used to trace these changes in the WM composition (Table 2). From these results it is possible to determine that during the solidification of the welded metal it has been produced the depletion of the dendrite cores in Cr and Mo and the increase of the content of these elements in the grain boundaries. In fact, the grain boundaries contain an extra 2.11 % Cr and 15.08 % Mo relative to the dendrite cores. That is, welding causes variations in the BM microstructure regarding not only grain morphology but also composition. Because of the segregation problem in highly alloy austenitic stainless steels [36], such as Alloy 31 (BM), a normal industrial practice is welding these materials using nickel-base filler metals with high molybdenum content, like the filler metal used in this work (Alloy 59).

Table 2. EDX (wt%) analysis of WM

	Chromium	Molybdenum
Bulk	24.02	13.05
Dendrite cores	23.35	11.43
Grain boundary	25.46	26.51

3.2. Open Circuit Potential measurements

The complete register of the open circuit potential measured for one hour at 25, 40, 60 and 80° C is shown in Figure 2 for the BM as an example. As can be seen, the potential increased during the first minutes of the test and stabilised with time. This behaviour was observed in BM, HAZ and WM, indicating that they have a good passive behaviour in phosphoric acid at the different temperatures studied. During the open circuit potential tests no change was observed on the surface of the working electrode at different temperatures, corroborating that the material was passivated at the different temperatures studied.

The OCP values of the three materials at the studied temperatures are summarised in Table 3. All the values are between 146 mV and 346 mV, corresponding to the passive region of the alloys in

this solution, as it will be discussed below. No clear tendency was observed in the OCP values of the different materials at the studied temperatures.

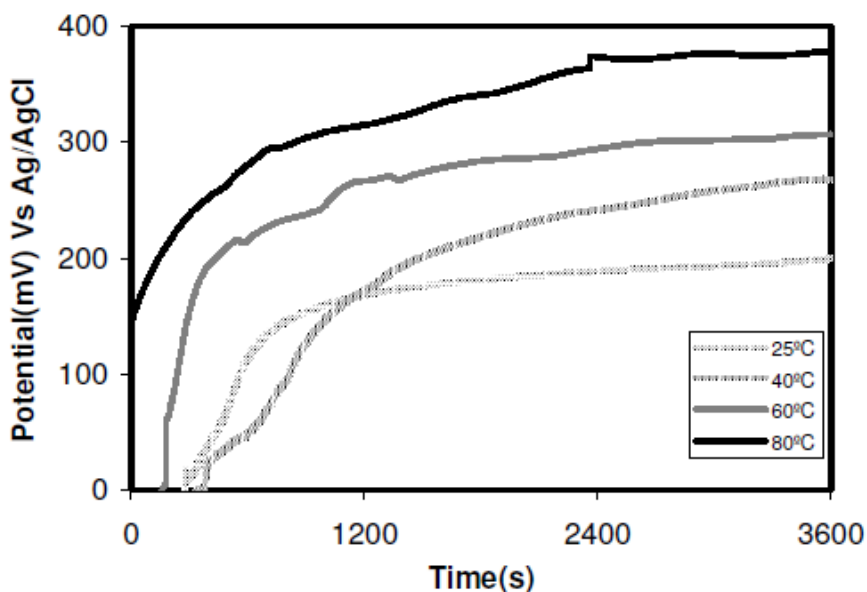


Figure 2. Open Circuit Potential of BM recorded for 1 hour at 25, 40, 60 and 80°C.

Table 3 shows that the OCP values increased with temperature, thus, it can be expected that temperature enhances not only the kinetics of the corrosion reaction [1, 37, 38], but also the kinetics of the passivation one.

Table 3. Open Circuit Potential values of the different alloys in the polluted phosphoric acid solution.

	OCP (mV _{Ag/AgCl})			
	25°C	40°C	60°C	80°C
BM	146	267	305	331
HAZ	142	212	329	338
WM	165	282	316	346

The displacement of OCP towards more positive values with temperature (Table 3) was justified by the passive nature of the alloys under study. During the OCP test the passive film grew on the electrode surface, shifting the OCP value to higher potentials [39]. It is well known that temperature favours the kinetics of corrosion reactions [40-43] however it also promotes the fast growth of passive films on metallic surfaces [44-46] which causes the ennoblement of the metal. On the other hand, the increase in OCP values with time during immersion in the studied polluted

phosphoric acid solutions at any temperature was attributable to the growth of the passive film [47]. This growth continues until the passive film acquires a thickness that is stable in the electrolyte.

Alloy 31 contains 26.75% chromium, chromium oxide being considered the main passive component of the passive film in the anodic polarisation of stainless steels [3]. On the other hand, phosphoric acid media favour the formation of iron phosphates[48].

Phosphate species can precipitate with dissolved iron species to form iron phosphates, since these compounds are characterised by a low solubility. Precipitation of iron phosphate occurs at the metal-solution interface [49, 50]. Building up the phosphate layer and passivation of the metal are similar to the model proposed by Bouchemel [51] for titanium-copper alloys in phosphate solutions. Wang and Turner [52] are also according with the fact that phosphate is able to incorporate into the passive film during the passivation process.

Comparison of the OCP values obtained in the previous work of the authors developed in 5.5 M phosphoric acid solution without impurities [19], with the OCP values obtained in the polluted solution (0.03 wt% of chloride ions and 2 wt% of H₂SO₄), shows lower values in the polluted solution than in the pure one in all the range of temperatures studied. This fact can be due to the fact that the impurities could be adsorbed on the metal surface, modifying the properties of the passive film and making it less protective [53].

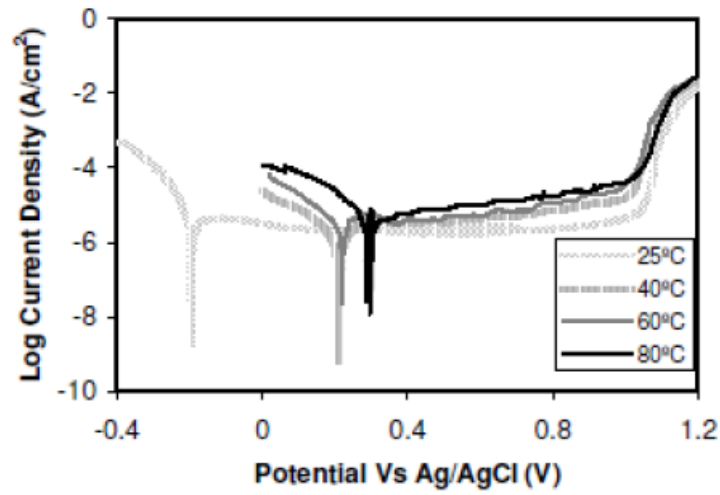
3.3. Potentiodynamic polarisation curves and electrochemical parameters

Figure 3 shows the potentiodynamic curves of BM, HAZ and WM in 5.5 M polluted phosphoric acid solutions at different temperatures, those are typical of passive materials. These materials were spontaneously passivated in the studied polluted phosphoric acid solutions at 25, 40, 60 and 80° C, as the OCP values (Table 3) found in the passive zone of the potentiodynamic curves (Figure 3) show.

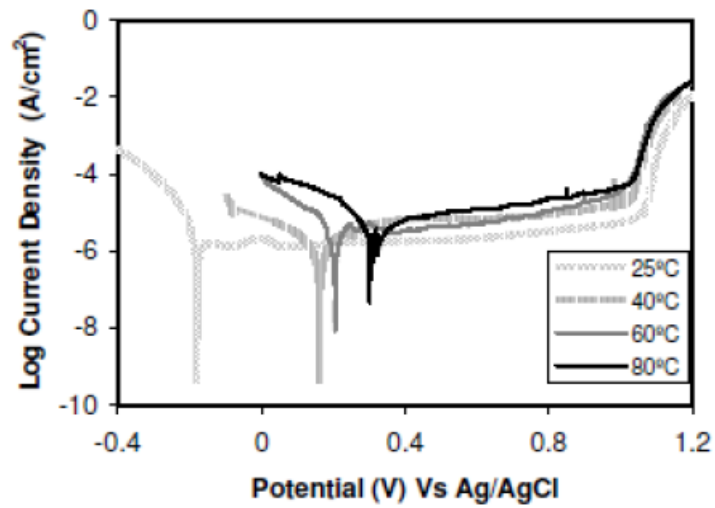
The E_{corr} and i_{corr} values, parameters characteristic of the corrosion resistance of the materials, were obtained from the potentiodynamic curves (Figure 3) and are shown in Table 4.

Table 4. Corrosion potentials (E_{corr} (mV_{Ag/Ag/Cl})) and corrosion current densities (i_{corr} (μA/cm²)) at different temperatures in the polluted Phosphoric Acid solution.

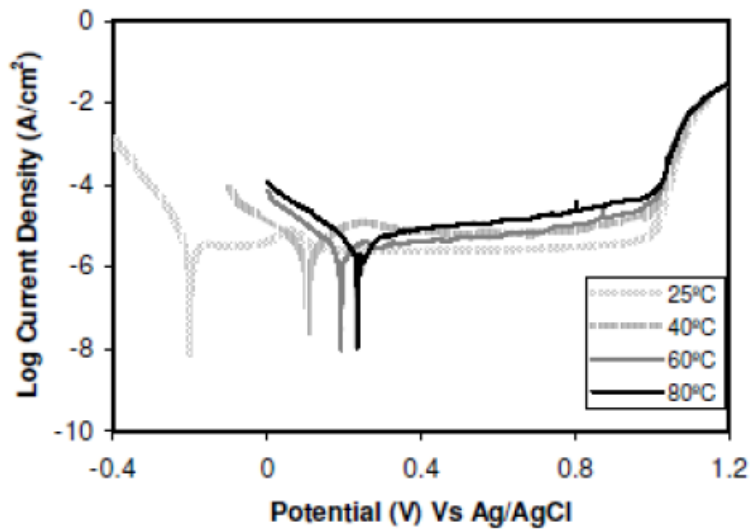
Materials	25°C		40°C		60°C		80°C	
	E_{corr} (mV)	i_{corr} (μA/cm ²)	E_{corr} (mV)	i_{corr} (μA/cm ²)	E_{corr} (mV)	i_{corr} (μA/cm ²)	E_{corr} (mV)	i_{corr} (μA/cm ²)
BM	-197	3.31	210	0.94	220	2.64	298	2.80
HAZ	-179	3.04	163	1.07	205	2.02	315	1.90
WM	-201	3.10	106	2.03	192	2.96	235	1.82



(a)



(b)



(c)

Figure 3. Potentiodynamic curves of BM (a), HAZ (b) and WM (c) in the 5.5 M polluted phosphoric solution at 25, 40, 60 and 80°C.

The E_{corr} (Table 4) shifted towards more positive values as temperature increased. This increase seems to be related with the increase in cathodic current densities with temperature, which shifts the corrosion potentials to higher values [38, 54]. The corrosion potentials followed the same tendency as the OCP values, but they are lower. This phenomenon was justified because during the open circuit measurements a protective oxide film was formed on the metal surface, shifting the potential to nobler values [32].

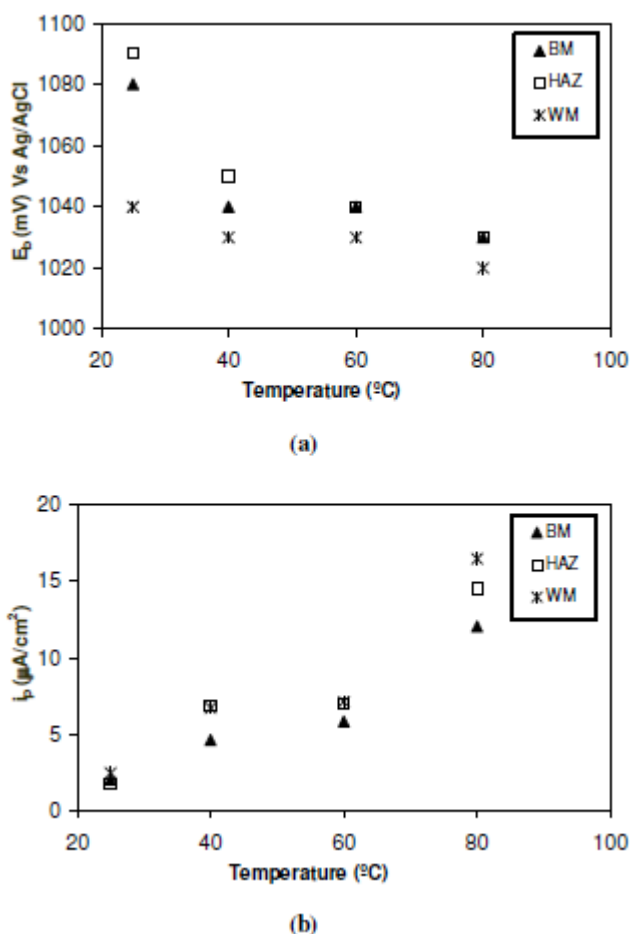


Figure 4. (a) Breakdown Potentials (E_b (mV_{Ag/AgCl})) and (b) Passivation Current Densities (i_p ($\mu\text{A}/\text{cm}^2$)) of the materials at different temperatures in the polluted phosphoric acid solution.

The WM showed more active E_{corr} values than BM and HAZ at all studied temperatures (Table 4). This can be attributed to the segregation of alloy elements, particularly Cr and Mo, during the solidification process, as it was detected in the EDX analysis of the WM (Table 2). This fact causes a decrease in their corrosion resistance, which in turn results in more active corrosion potential values [55-57] (Table 4).

The i_{corr} (Table 4) values did not show a clear trend with temperature. At 25°C and 80°C, the highest values were obtained for BM, while at 40°C and 60°C, the highest values of i_{corr} were obtained for WM.

Figure 4 shows the E_b and i_p values of the materials at the different temperatures under study in the polluted phosphoric acid solution. It was observed a decrease of the E_b values (Figure 4a) and an increase of the i_p values (Figure 4b) with temperature. These i_p values were not lower than their corresponding corrosion current densities, although the three materials presented a stable passivation range at all the studied conditions. The WM presents the lowest E_b (Figure 4a) and, both HAZ and WM register the highest i_p values (Figure 4b). This fact indicates that the welding process modifies the characteristics of the passive film, deteriorating them and favouring the loss of passivity with respect to the BM. Some authors have attributed the loss of passivity of the welded metal to the presence of segregation products in the solidified welds [55, 57-59].

Comparing the E_b values obtained in this polluted 5.5 M phosphoric acid solution with the solution without impurities used in a previous work by the authors [19], it has been observed that the E_b values obtained in the polluted solution are lower than those obtained in the pure solution at any temperature. This behaviour could be attributed to the strong chemisorption of the chloride anions on the passive surface of the metal, making the breakdown of the passive film easier [60]. However, the i_p values obtained in the polluted solution were lower than those registered in the pure solution at any temperature. The passivation capability of sulphates, that are present in the polluted solution, observed by Abed [61] could explain this fact.

The difference between the breakdown potential and the corrosion potential ($E_b - E_{corr}$) corresponds to the passivation range, and it is a measure of the passivity of the materials. The greater the ($E_b - E_{corr}$) difference, the wider the range of potentials in which the metal remains passive. Figure 5 shows the passivation ranges of the three materials in the studied polluted phosphoric acid solutions at different temperatures. The passivation range decreased as temperature increased [62], since E_{corr} values increased and E_b decreased with temperature. The increment in temperature causes the loss of passivity to start earlier, which means lower passivation ranges [62]. Differences between the ($E_b - E_{corr}$) values of the different materials at each temperature were negligible.

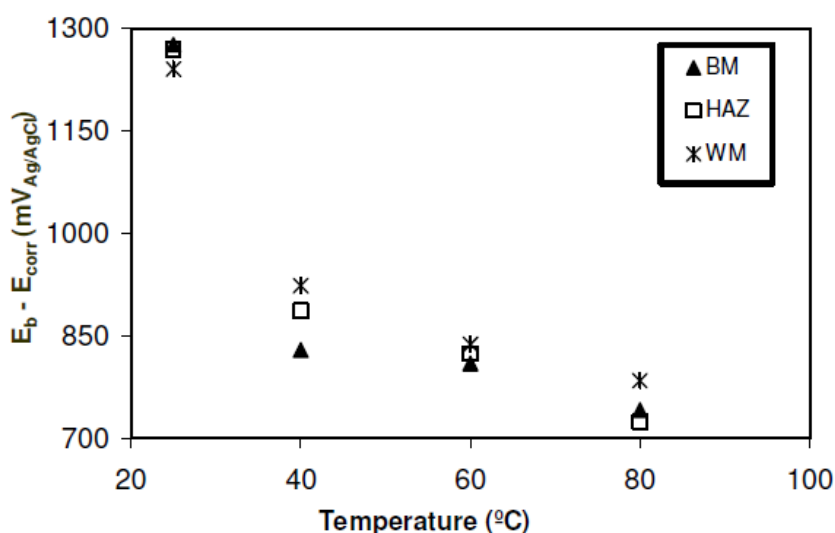


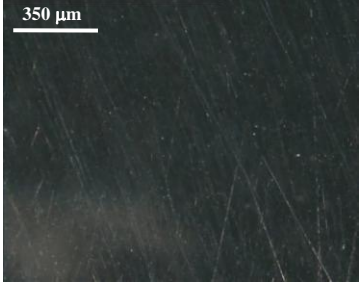
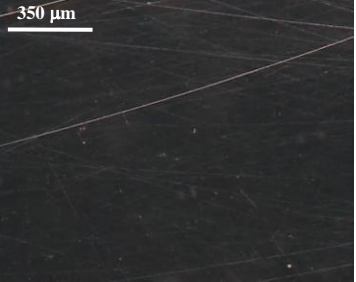
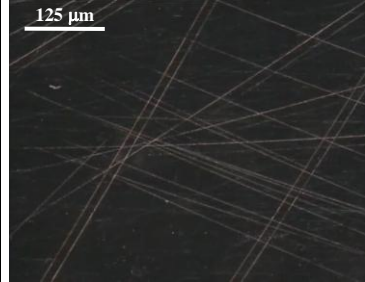
Figure 5. Passivation ranges in the polluted Phosphoric Acid solution.

The lower E_b and $(E_b - E_{corr})$ values and the higher i_p values obtained as temperature increases, reveal that the properties of the passive film formed degraded with temperature.

Results obtained in this work indicate that the passive films formed at lower temperatures are significantly less defective and more resistant to film breakdown or loss of passivity than those formed at higher temperatures, as reported by several authors [45, 52, 63, 64]. In this sense, Hur and Park [45] suggested that important changes in the composition of the films with increasing temperature are responsible for this decrease in the protective properties of the films formed at high temperatures. An increase in porosity is other of the main changes in film properties with increasing temperature, porosity being a potential factor leading to poorer protectiveness of the film [65]. An increase in temperature can also cause some intrinsic modifications in the chemical and/or physical structure of the passive film, resulting in a variation in the density of vacancies of them [52]. In other words, an increase in temperature causes the film to become thicker but more porous and then less protective [66] which can explain the decrease of the breakdown potential (Figure 4a) and of the passivation range (Figure 5) and the increase of the passivation current density (Figure 4b) with temperature. Similar results have been reported by several authors [37, 67].

Each material exhibits different morphologies of corrosion as result of the imposition of potential that takes place in the potentiodynamic curves. An example is shown in the Figure 6. This figure shows images of the BM, HAZ, and WM at different potentials at 60°C.

These images were obtained simultaneously to the electrochemical data acquisition using a device that consists of two elements: the electrochemical unit and the image acquisition section [21, 22]. The morphology of the attack of the BM and HAZ was similar at different temperatures. Figure 6 shows the electrode surface of the BM (Image A), HAZ (Image B) and WM (Image C) at the initial potential of the potentiodynamic sweep. The following images show the first signs of corrosion for BM (Image D), HAZ (Image E) and WM (Image F) at values above the breakdown potential, which was about 1030mV at 60°C for the three materials. Images G, H and I show how corrosion progressed uniformly.

BM	HAZ	WM
		
<p>A. E=-400mV Initial test</p>	<p>B. E=-400mV Initial test</p>	<p>C. E=-400mV Initial test</p>

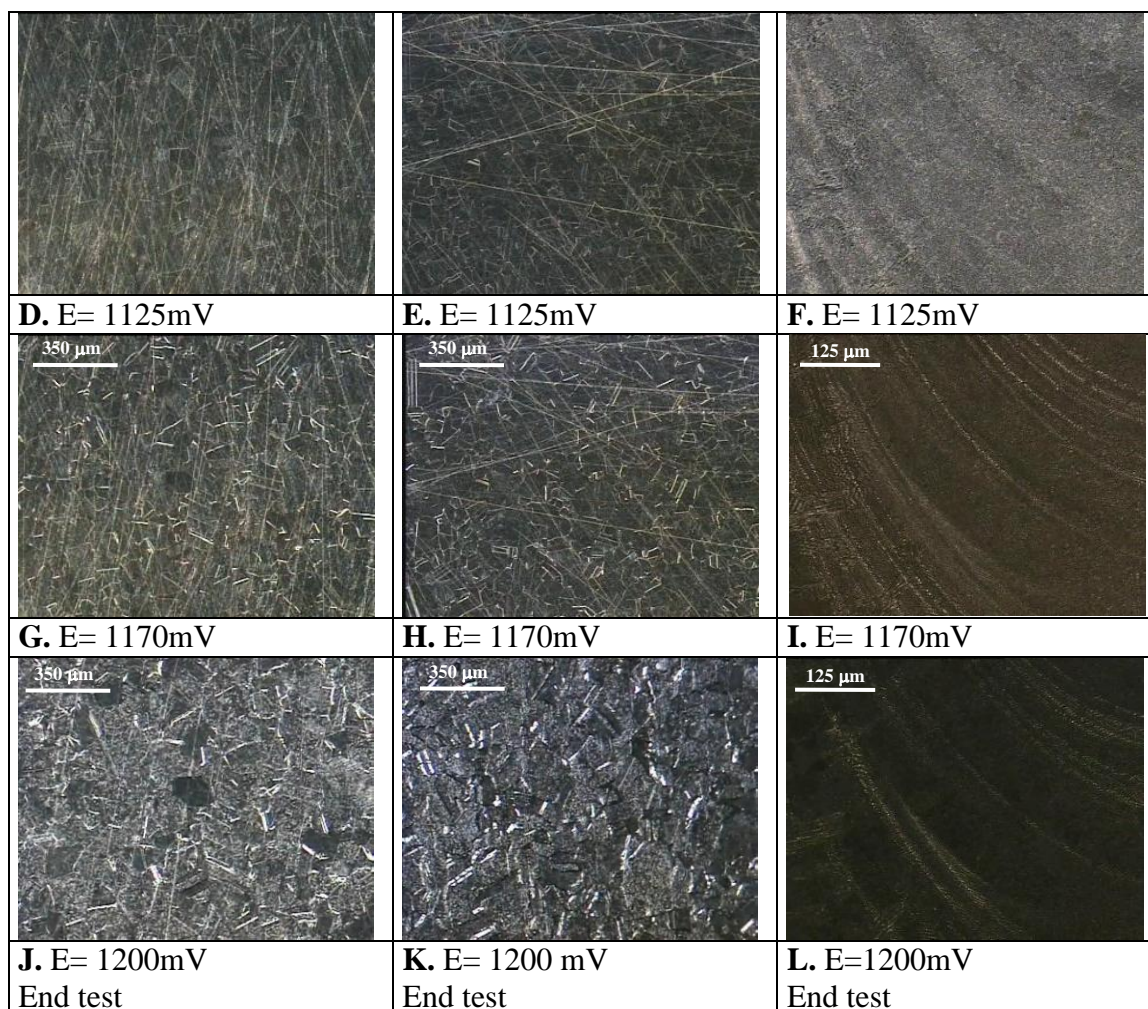


Figure 6. Images of BM, HAZ and WM at different potentials of the potentiodynamic test at 60 °C in polluted phosphoric solution.

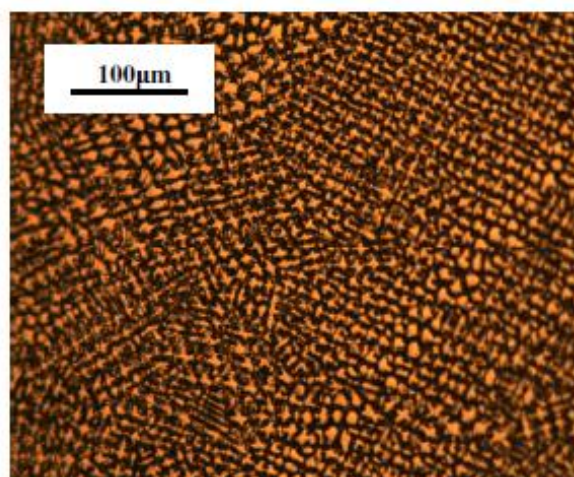


Figure 7. Image of WM after the potentiodynamic test at 60 °C in the polluted phosphoric solution.

At the end of the potentiodynamic sweep the surface of the electrode was completely corroded and it was possible to distinguish the austenitic grains in BM (Figure 6, Image J) and HAZ (Figure 6, Image K). Image L (40x) does not allow distinguish the microstructure of the WM, however an image taken at higher magnifications (100x) after the test (Figure 7) allows distinguish the dendrites typical of the WM.

3.4. Galvanic corrosion

Table 5 shows the mixed potential and the galvanic current density values obtained according to the mixed potential theory [24], as well as the differences between the corrosion potentials of the cathodic and the anodic part of the pairs (E_C-E_A) and the i_G/i_{corr} ratio, where i_{corr} is the corrosion current density of the uncoupled anode.

Table 5. Galvanic parameters in the polluted Phosphoric Acid solution. Letters A and B indicate the anode and cathode of the pair.

25 °C		
	BM (A)-HAZ (C)	HAZ (C)-WM (A)
E_M (mV _{Ag/AgCl})	-188	-188
E_C-E_A (mV _{Ag/AgCl})	18	22
i_G (μA/cm ²)	1.48	1.48
i_G/i_{corr}	0.45	0.48
40 °C		
	BM (C)-HAZ (A)	HAZ (C)-WM (A)
E_M (mV _{Ag/AgCl})	188	122
E_C-E_A (mV _{Ag/AgCl})	47	57
i_G (μA/cm ²)	1.26	1.85
i_G/i_{corr}	1.34	0.91
60 °C		
	BM (C)-HAZ (A)	HAZ (C)-WM (A)
E_M (mV _{Ag/AgCl})	214	196
E_C-E_A (mV _{Ag/AgCl})	15	13
i_G (μA/cm ²)	1.22	1.05
i_G/i_{corr}	0.47	0.5
80 °C		
	BM (A)-HAZ (C)	HAZ (C)-WM (A)
E_M (mV _{Ag/AgCl})	300	284
E_C-E_A (mV _{Ag/AgCl})	17	80
i_G (μA/cm ²)	1.71	4.30
i_G/i_{corr}	0.61	2.36

With respect to the BM-HAZ pair, BM is the anode of the pair at 25°C and 80°C, while it is the cathode at 40°C and 60°C. This behaviour could be attributed to the similar microstructure of both materials, equiaxed austenitic grains, which means that the thermal effect is not very significant on the HAZ microstructure. Therefore, the variation in the polarity of the BM-HAZ pair could be due to any change in the working conditions, medium conditions or temperature [30, 68]. In the case of the HAZ-WM pairs, WM is the anode at any temperature, which has been attributed to the segregation of the alloying elements during solidification (Table 2). Therefore, the corrosion resistance of the welded metal decreases due to the galvanic effect produced in the weld at all the studied temperatures.

Similarly to the corresponding corrosion potentials of the uncoupled materials, Table 5 shows that E_M have the same tendency to shift to more noble values as temperature increases. Minimal differences of 100-130 mV between the corrosion potential of the cathode and the anode of the pair ($E_C - E_A$) are necessary to consider the galvanic effect significant [69]. Table 5 shows that, the ($E_C - E_A$) values are lower than 100 mV at all the temperatures studied, therefore the galvanic effect on the BM-HAZ and HAZ-WM pairs seems not to be significant.

On the other hand, the i_G values do not follow a clear tendency with temperature, as it was observed with the i_{corr} of each part of the pairs. According to Mansfeld and Kendel [70], the relative increase in the corrosion rate of the anode of the galvanic pair could be expressed by the i_G/i_{corr} ratio, where i_{corr} is the corrosion current density of the uncoupled anode. The magnitude of this ratio may be used as a guide to reflect the severity of the galvanic effect, and it was suggested that a i_G/i_{corr} value lower than 5 means compatibility of the parts in a galvanic pair [71]. Table 5 shows that the i_G/i_{corr} values are lower than 3, even in any case this value is lower than 1, indicating that the corrosion rate of the anode is lower when it is coupled than when it is uncoupled. Therefore, it can be concluded that the BM-HAZ and HAZ-WM pairs are compatible when they form galvanic pairs, which is also in agreement with the low difference ($E_C - E_A$).

4. CONCLUSIONS

BM, HAZ and WM spontaneously passivated in the 5.5 M polluted phosphoric acid solutions at 25, 40, 60 and 80° C, as shown by the OCP values and the potentiodynamic curves registered in this work.

The lower E_b and ($E_b - E_{corr}$) values and the higher i_p values obtained as temperature increases, indicate that the properties of the passive film formed degraded with temperature.

The welding process modifies the characteristics of the passive film, deteriorating them and favouring the loss of passivity of WM with respect to BM, as the lowest E_b values and highest i_p values of the WM demonstrated.

The surface of the materials degraded uniformly during the corrosion process, which means uniform corrosion of the materials in the 5.5 M polluted phosphoric acid solutions at the studied temperatures.

The BM-HAZ and HAZ-WM pairs are compatible when they form galvanic pairs in the 5.5 M polluted phosphoric acid solutions at the studied temperatures, as demonstrated by the low (E_C-E_A) and i_G/i_{corr} values.

ACKNOWLEDGMENTS

We wish to express our gratitude to the Ministerio de Asuntos Exteriores y Cooperación of Spain (PCI Mediterráneo C/8196/07, C/018046/08, D/023608/09, D/030177/10), to Universidad Politécnica de Valencia (PAID-06-09), to Generalitat Valenciana (GV/2011/093) and to Dr. Asuncion Jaime for her translation assistance.

References

1. P. Becker, *Phosphates and Phosphoric Acid. Raw Materials, Technology, and Economics of the Wet Process*, T.P.Hignett and D.A.Palgrave, (eds.), New York, 1989.
2. A.Bellaouchou, A. Guenbour, A. Benbachir, *Corrosion* 49 (1993) 656.
3. H. Iken, R. Basseguy, A. Guenbour, A. Benbachir, *Electrochim. Acta* 52 (2007) 2580.
4. S. El Hajjaji, L. Aries, J. P. Audouard, F. Dabosi, *Corros. Sci.* 37 (1995) 927.
5. M. Honda, S. Kobayashi, *Mater. Performance* 33 (1994) 66.
6. A.Guenbour, M. A. Hajji, E. M. Jallouli, A. Benbachir, *Appl. Surf. Sci.* 253 (2006) 2362
7. H. A. El Dahan, *J. Mater. Sci.* 34 (1999) 851
8. E. Sarmiento, J. G. González-Rodríguez, J. Uruchurtu, O. Sarmiento, M. Menchaca, *Int. J. Electrochem. Sci.* 4 (2009) 144.
9. M. T. Montañés, R. Sánchez-Tovar, J. García-Antón, V. Pérez-Herranz, *Int. J. Electrochem. Sci.* 5 (2010) 1934.
10. S. A. M. Refaey, F. Taha, A. M. Abd El-Malak, *Int. J. Electrochem. Sci.* 1 (2006) 80.
11. A.S. Hamdy, E. El-Shenawy, T. El-Bitar, *Int. J. Electrochem. Sci.* 1 (2006) 171.
12. D. M. García-García, E. Blasco-Tamarit, J. García-Antón, *Int. J. Electrochem. Sci.* 6 (2011) 1237
13. R. Leiva-García, M. J. Muñoz-Portero, J. García-Antón, *Int. J. Electrochem. Sci.* 6 (2011) 442
14. J. Mendoza-Canales, J. Marín-Cruz, *Int. J. Electrochem. Sci.* 3 (2008) 346.
15. A.Y. Musa, A. A. H. Kadhum, A. Bakar-Mohamad, A. Razak-Daud, M. Sobri-Takriff, S. Kartom-Kamarudin, N. Muhamad, *Int. J. Electrochem. Sci.* 4 (2009) 707.
16. M. Dadfar, M. H. Fathi, F. Karimzadeh, M. R. Dadfar, A. Saatchi, *Mater. Lett.* 61 (2007) 2343
17. B. Brunton, *Materials Australia* 29 (1997) 14
18. R. Sánchez-Tovar, M. T. Montañés, J. García-Antón, *Corros. Sci.* 52 (2010) 1508
19. E. Blasco-Tamarit, D. M. García-García, M. Ibáñez-Ferrándiz, J. García-Antón, A. Guenbour, *Corrosion* 67 (2011) 035001-1
20. ASTM G-5, Test Method for Making Potentiostatic and Potentiodynamic Anodic Polarisation Measurements, 2004.
21. J. García-Antón, A. Igual-Muñoz, J. L. Guiñón, V. Pérez-Herranz, Spain, P-200002525 (2000).
22. J. García-Antón, A. Igual-Muñoz, J. L. Guiñón, V. Pérez-Herranz, Spain, P-200002526 (2000).
23. ASTM G-3, Standard Practice for Conventions Applicable to Electrochemical Measurements in Corrosion Testing, 2010.
24. C. Wagner, *J. Electrochem. Soc.* 98 (1951) 116
25. N. Pérez, *Electrochemistry and corrosion science*, Kluwer Academic, (ed.), USA, 2004.
26. H. P. Hack, *Evaluation of galvanic corrosion, Corrosion: Fundamentals, Testing and Protection*, vol 13A, in: ASM International (ed.), ASM Handbook, 2003.
27. L. Reclaru, R. Lerf, P. Y. Eschler, A. Blatter, J. M. Meyer, *Biomaterials* 23 (2002) 3479
28. F. Mansfeld, Z. Sun, C. H. Hsu, A. Nagiub, *Corros. Sci.* 43 (2001) 341

29. L. Reclaru, R. Lerf, P. Y. Eschler, J.-M. Meyer, *Biomaterials* 22 (2001) 269
30. E. Blasco-Tamarit, A. Igual-Muñoz, J. García-Antón, D. García-García, *Corros. Sci.* 50 (2008) 3590
31. E. Blasco-Tamarit, A. Igual-Muñoz, J. García-Antón, D. García-García, *Corros. Sci.* 49 (2007) 1000
32. E. Blasco-Tamarit, A. Igual-Muñoz, J. García-Antón, *Corros. Sci.* 49 (2007) 4452
33. E. Blasco-Tamarit, A. Igual-Muñoz, J. García-Antón, D. García-García, *Corros. Sci.* 48 (2006) 863
34. G. F. Vander Voort, *Metallography: Principles and Practice*, ASM International, (ed.), 1999.
35. *Metallography and Microstructures*, ASM Handbook vol 9, ASM International, (ed.), 2004.
36. Tsung-Yuan Kuo, Hwa-Teng Lee, *Mater. Sci. Eng. A* 338 (2002) 202
37. A. Guenbour, H. Iken, N. kebkar, A. Bellaouchou, R. Boulif, A. Benbachir, *Appl. Surf. Sci.* 252 (2006) 8710
38. R. Sánchez-Tovar, M. T. Montañés, J. García-Antón, A. Guenbour, A. Benbachir, Corrosion behaviour of micro-plasma arc welded stainless steels in H₃PO₄ under flowing conditions at different temperatures, *Corros. Sci.* 53 (2011) 1237-1246
39. G. Lothongkum, S. Chaikittisilp, A. W. Lothongkum, *Appl. Surf. Sci.* 218 (2003) 202
40. A. Igual-Muñoz, J. García-Antón, S. López Nuévalos, J. L. Guiñón, V. Pérez-Herranz, *Corros. Sci.* 46 (2004) 2955
41. A. Pardo, E. Otero, M. C. Merino, M. D. López, M. V. Utrilla, F. Moreno, *Corrosion* 56 (2000) 411
42. N. J. Laycock, *Corrosion* 55 (1999) 590
43. L. F. Garfias-Mesias, J. M. Sykes, *Corros. Sci.* 41 (1999) 959
44. A. Igual-Muñoz, J. García-Antón, J. L. Guiñón, V. Pérez-Herranz, *Corros. Sci.* 48 (2006) 3349
45. D. H. Hur, Y. S. Park, *Corrosion* 62 (2006) 745
46. C. O. A. Olsson, D. Landolt, *Electrochim. Acta* 48 (2003) 1093
47. E. A. Abd El Meguid, A. A. Abd El Latif, *Corros. Sci.* 49 (2007) 263
48. M. Reffass, R. Sabot, M. Jeannin, C. Berziou, P. H. Refait, *Electrochim. Acta* 54 (2009) 4389
49. E. Almeida, D. Pereira, M. O. Figueiredo, V. M. Lobo, M. Morcillo, *Corros. Sci.* 39 (1997) 1561
50. S. R. Moraes, D. Huerta-Vilca, A. J. Motheo, *Prog. Org. Coat.* 48 (2003) 28
51. H. Bouchemel, A. Benchettara, *Mater. Chem. Phys.* 115 (2009) 572
52. H. Wang, J. A. Turner, *J. Power Sourc.* 180 (2008) 803
53. P. Marcus, *J. Chim. Phys. Phys.- Chim. Biol.* 88 (1991) 1697
54. E. Blasco-Tamarit, A. Igual-Muñoz, J. García-Antón, D. García-García, *Corros. Sci.* 50 (2008) 1848
55. P. I. Marshall, T. G. Gooch, *Corrosion* 49 (1993) 514
56. T. Hemmingsen, H. Hovdan, P. Sanni, N. O. Aagotnes, *Electrochim. Acta* 47 (2002) 3949
57. [57] G. Madhusudhan Reddy, A. A. Gokhale, N. Narendra Janaki Ram, K. Prasad Rao, *Br. Corros. J.* 36 (2001) 304
58. Y. Cui, C. D. Lundin, *Mater. Lett.* 59 (2005) 1542
59. Y. Cui, C. D. Lundin, *Mater. Des.* 28 (2007) 324
60. M. A. M. Ibrahim, S. S. Abd El Rehim, M. M. Hamza, *Mater. Chem. Phys.* 115 (2009) 80
61. Y. Abed, B. Hammouti, *Bull. Electrochem.* 16 (2000) 296
62. A. Neville, T. Hodgkiess, *Corros. Sci.* 38 (1996) 927
63. P. E. Manning, D. J. Duquette, *Corros. Sci.* 20 (1980) 597
64. Z. Szklarska-Smialowska, *Corrosion* 30 (1974) 161.
65. T. Laitinen, N. Bojinov, I. Betova, K. Mäkelä, T. Saario, *The properties of and transport phenomena in oxide films on iron, nickel, chromium and their alloys in aqueous environments*, Publication of STUK (Radiation and nuclear safety authority Finland) (1999) 1-75.
66. J. H. Wang, C. C. Su, Z. Szklarska-Smialowska, *Corrosion* 44 (1988) 732

67. J. Charles, D. Catelin, F. Dupouiron, *Mater. Technol.* 8 (1987) 309
68. C. García, F. Martín, P. de Tiedra, Y. Blanco, M. López, *Corros. Sci.* 50 (2008) 1184
69. E. Otero Huerta, *Corrosion and Materials Degradation*, Síntesis, (ed.), Madrid, 1997.
70. F. Mansfeld, J. V. Kendel, *Laboratory studies of galvanic corrosion of aluminium alloys.*, in: R.Raboian, W.D.France (eds.), *Galvanic and Pitting Corrosion-Field and Laboratory Studies*, ASTM STP 576, ASTM, 1976, 20-47.
71. F. T. Cheng, K. H. Lo, H. C. Man, *Surf. Coat. Technol.* 172 (2003) 316